Progress in additive manufacturing of pure tungsten for plasma-facing component applications

A. v. Müller[a], D. Dorow-Gerspach[b], M. Balden[a], M. Binder[c], B. Buschmann[c], B. Curzadd[a,d], T. Loewenhoff[b], R. Neu[a,d], G. Schlick[c], J.H. You[a]

[a] *Max-Planck-Institut für Plasmaphysik, 85748 Garching, Germany*
[b] *Forschungszentrum Jülich, 52425 Jülich, Germany*
[c] *Fraunhofer IGCV, 86153 Augsburg, Germany*
[d] *Technische Universität München, 85748 Garching, Germany*

Abstract

In the present paper, recent progress regarding *additive manufacturing* (AM) of pure tungsten (W) by means of *laser powder bed fusion* (LPBF) is discussed. In this context, several aspects are highlighted: The influence of the raw powder material characteristics on the resulting W part quality is briefly discussed, examples for complexly shaped additively manufactured W lattice structure samples are shown, the application of an additively manufactured W structure as preform for a tungsten-copper (W-Cu) composite is illustrated and thermal shock experiments on additively manufactured bulk W samples with the electron beam facility JUDITH 2 are described. The latter demonstrates that W material consolidated by means of LPBF is capable of surviving intense thermal shock loads. This is an encouraging result indicating that the thermal performance and stability of W fabricated by means of LPBF is comparable to that of conventionally fabricated W which in turn implies that the further investigation of additively manufactured W as candidate material with regard to applications in highly loaded *plasma-facing components* (PFCs) of future magnetic confinement thermonuclear fusion devices can be considered worthwhile.

Keywords: *additive manufacturing, refractory metal, tungsten, laser powder bed fusion, plasma-facing component*

1. Introduction

The term *additive manufacturing* (AM) describes fabrication processes with which three-dimensional objects are realised by means of sequential layerwise deposition of material under computer control. Therefore, objects with more or less arbitrary shape can be produced straightforwardly with such a fabrication technology. In this context, the field of AM of metals by means of *laser powder bed fusion* (LPBF) has developed rapidly during recent years [1, 2].

With respect to applications regarding magnetic confinement thermonuclear fusion reactors the AM of tungsten (W) is of interest since W is currently considered the preferred *plasma-facing material* (PFM) due to its high threshold energy for physical sputtering as well as its low retention of hydrogen isotopes [3]. Moreover, there is an increased interest in W containing composite materials for applications in highly loaded *plasma-facing components* (PFCs) which are components that have to sustain intense particle, heat and neutron fluxes during fusion operation [4, 5]. In this context, the AM of W could be beneficial with respect to the design of PFCs as conventional fabrication technologies for W products represent a limiting factor.

Previous studies [6, 7] demonstrated that pure W can be consolidated reasonably by means of LPBF processing. In this context, it was identified that a deposited energy density of approximately $250\,\mathrm{J\,mm^{-3}}$ for a laser power of 400 W together with a substrate preheating of 1000 °C represent reasonable manufacturing parameters. Apart from that, it was demonstrated that thin-walled W parts can be produced straightforwardly by means of LPBF. Nevertheless, W is a particularly challenging material for LPBF due to the combination of the high thermal gradients that occur during the LPBF process (spatial temperature gradients of approximately $1 \times 10^2\,\mathrm{K\,mm^{-1}}$ to $1 \times 10^4\,\mathrm{K\,mm^{-1}}$, cooling rates higher than $1 \times 10^4\,\mathrm{K\,s^{-1}}$ [2]) and the intrinsic properties of W. As a *body-centred cubic* (bcc) metal, W is a material with a particularly high *ductile-to-brittle transition temperature* (DBTT) and hence prone to the formation of microcrack defects during LPBF processing. It was shown that even a substrate preheating up to 1000 °C does not inhibit the formation of such microcrack defects [7]. In Figure 1, an image of the LPBF processing of pure W with preheated substrate is shown in order to illustrate such a fabrication of W parts by means of LPBF. In the present paper, recent progress regarding the AM of pure W by means of LPBF is reported. In more detail, the influence of the raw powder material characteristics on the resulting W part quality is briefly discussed and examples for complexly shaped additively manufactured W lattice structure samples are shown. Moreover, the application of an additively manufactured W structure

Corresponding author: Alexander v. Müller, alexander.v.mueller@ipp.mpg.de

as preform for a tungsten-copper (W-Cu) composite is illustrated. Such composite structures could potentially serve as optimised PFC heat sinks with tailored W-Cu material distribution. Furthermore, thermal shock experiments on additively manufactured bulk W samples are described.

Figure 1: LPBF processing of pure W with a preheated substrate; the round subtrate plate (diameter 200 mm) as well as the parts being fabricated can be identified within the powder bed due to the annealing colour.

2. Effects of raw powder material quality

In most published studies regarding LPBF of W, mainly the effects of laser exposure parameters on the material quality of consolidated W were investigated [6, 7, 8, 9, 10, 11, 12, 13, 14, 15, 16]. However, it is known that the characteristics of the raw powder material have a significant influence on the process stability and quality of the consolidated material in powder bed based AM processes like LPBF. Hence, this aspect was investigated for W in more detail [17] and is highlighted within this section. Several powder characteristics are decisive for powder bed based AM processes. Primarily important are, however, the powder particle morphology as well as the *particle size distribution* (PSD) of the powder. These two parameters typically determine to a large extent the flowability of a powder as well as the resulting powder bed density during LPBF processing. A good flowability is of paramount importance in powder bed based AM processes for a consistent layer formation. In this context, the desired morphology of powder particles is spherical. Further powder characteristics are e.g. the chemical composition or optical properties that determine the absorption of the laser beam power. All these powder characteristics eventually result in a specific behaviour during the LPBF process through a complex interplay of physicochemical phenomena that finally determine the quality of a material consolidated during the LPBF process.

In Figure 2, *scanning electron microscopy* (SEM) images of three different W powders that were investigated regarding their processability through LPBF are illustrated. Figure 2a shows a spheroidised W powder with almost only round and comparably small particles (supplier: Tekna Advanced Materials Inc., product name: W -25). Figure 2b shows a partly spheroidised W powder (supplier: Global Tungsten & Powders Corp., product name: WD 200) in which the particle morphology ranges from completely spheroidised to polygonal. Eventually, Figure 2c shows a rather standard polygonal W powder (supplier: H.C. Starck GmbH, product name: HC 4000) with comparably large particles.

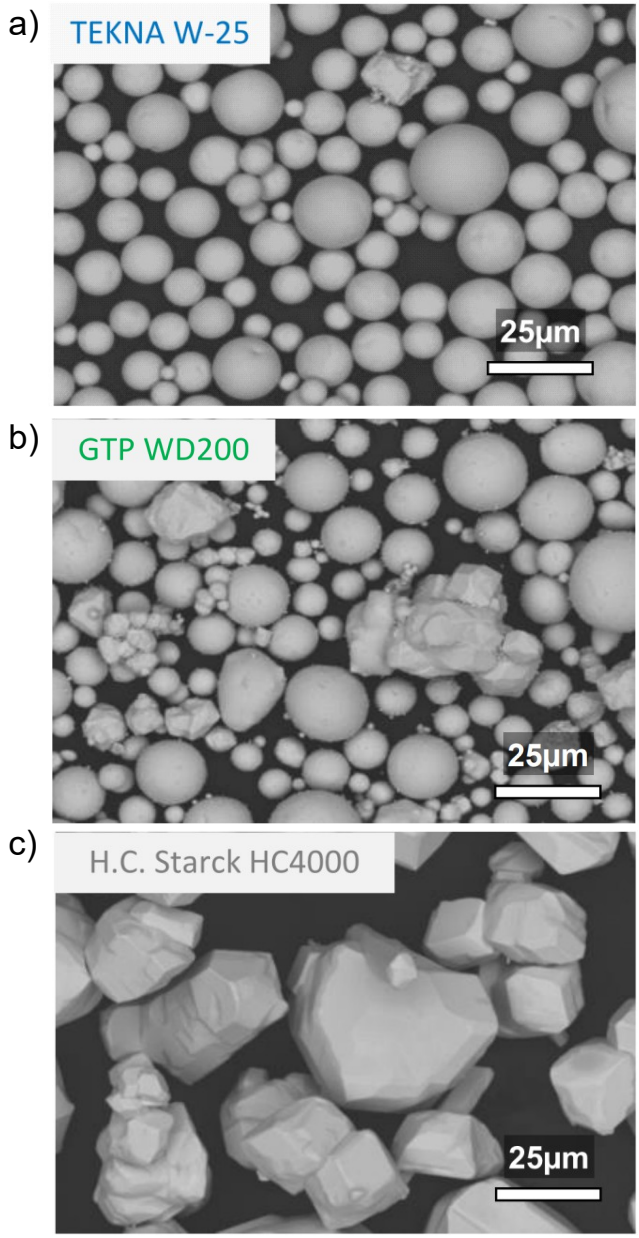

Figure 2: SEM images of three investigated W powders; (a) spheroidised W powder (supplier: Tekna Advanced Materials Inc., product name: W -25), (b) partly spheroidised W powder (supplier: Global Tungsten & Powders Corp., product name: WD 200) as well as (c) polygonal W powder (supplier: H.C. Starck GmbH, product name: HC 4000).

In Figure 3, the PSD of the three W powders illustrated in Figure 2 is depicted. The particle sizes are given in micrometer on the abscissa while the share of volume regarding the respective particle size is given on the ordinate in percent. The PSDs were measured by means of laser diffraction with a *Mastersizer 3000* by *Malvern Panalytica*. Figure 3 shows that, as expected, distinct

differences can be identified regarding the three investigated powders. The TEKNA W-25 powder exhibits a comparably sharp PSD while the other two investigated powders exhibit a broader distribution. The ploygonal W powder supplied by H.C. Starck exhibits the largest particle sizes as has also been observed in the SEM images illustrated in Figure 2.

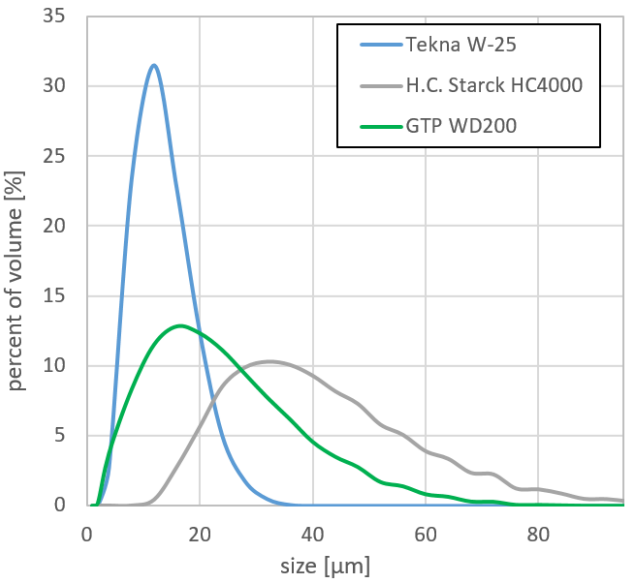

Figure 3: PSD of the three investigated W powders measured by means of laser diffraction.

Moreover, chemical composition analyses were performed on the investigated W powders. Carbon (C), sulphur (S), oxygen (O), nitrogen (N) and hydrogen (H) contents were measured by means of combustion analyses that were performed with a *Leco CS 600* carbon/sulphur determinator as well as a *Leco TCH 600* nitrogen/oxygen/hydrogen determinator. In this context, O contaminations could be measured regarding all investigated W powders and are illustrated in Figure 4. Relevant levels with respect to the other analysed impurities (C, S, H, N) were not measured.

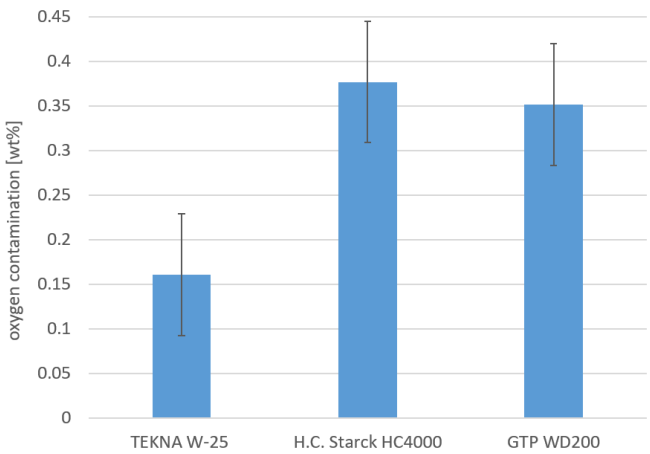

Figure 4: Oxygen contaminations of the three investigated W powders measured by means of combustion analyses.

In Figure 5, the unambiguous influence of the raw powder material characteristics on the quality of W parts fabricated by means of LPBF is illustrated. The SEM images in Figures 5b, 5c and 5d show the top and side views on additively manufactured test parts - a junction of three thin walls as illustrated in Figure 5a - that were fabricated with different raw powder materials but with the same laser exposure parameters as well as on the same LPBF facility (SLM 250 HL, located at Fraunhofer IGCV, 86159 Augsburg, Germany).

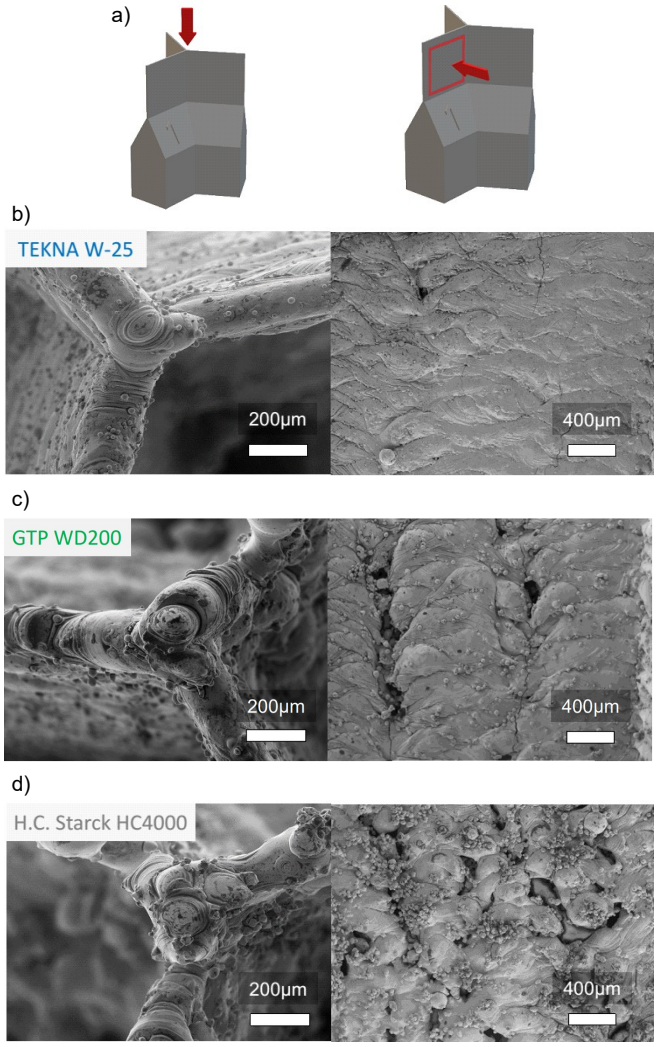

Figure 5: (a) Test part consisting of a junction of three thin walls; SEM images of top and side views on additively manufactured test parts that were fabricated with (b) spheroidised, (c) partly spheroidised and (d) polygonal W powders as illustrated in Figure 2.

The differences in built part quality that can be identified in Figures 5b, 5c and 5d are plainly visible and illustrate that there is a strong influence of the powder characteristics. It can be stated that the spherical W powder (Figure 5b, supplier: Tekna Advanced Materials Inc., product name: W -25) yields notably better results compared with the partly spheroidised W powder (Figure 5c, supplier: Global Tungsten & Powders Corp., product name: WD 200) as well as the polygonal W powder (Figure 5c, supplier: H.C. Starck GmbH, product name: HC 4000) especially in terms of porosity

and surface quality. The differences in built part quality illustrated in Figure 5 are evident. It should however be considered that the samples were fabricated with same laser exposure parameters meaning that the results could to some extent possibly be improved when LPBF conditions optimised for each powder are applied.

3. Complexly shaped tungsten parts

Examples for complexly shaped W samples are illustrated in Figure 6 which shows anisotropic W lattices that were built on an Aconity*ONE* LPBF facility, located at Fraunhofer IGCV, 86159 Augsburg, Germany. Spheroidised W powder as illustrated in Figure 2a (supplier: Tekna Advanced Materials Inc., product name: W -25) was used as raw material. Such lattice structures are currently being investigated with regard to plasma limiter components for a *DEMOnstration fusion reactor* (DEMO) [18, 19]. Figure 6a shows several samples on a W substrate plate after the LPBF process and powder removal. Figure 6b shows a microscopic top view on an additively manufactured W lattice.

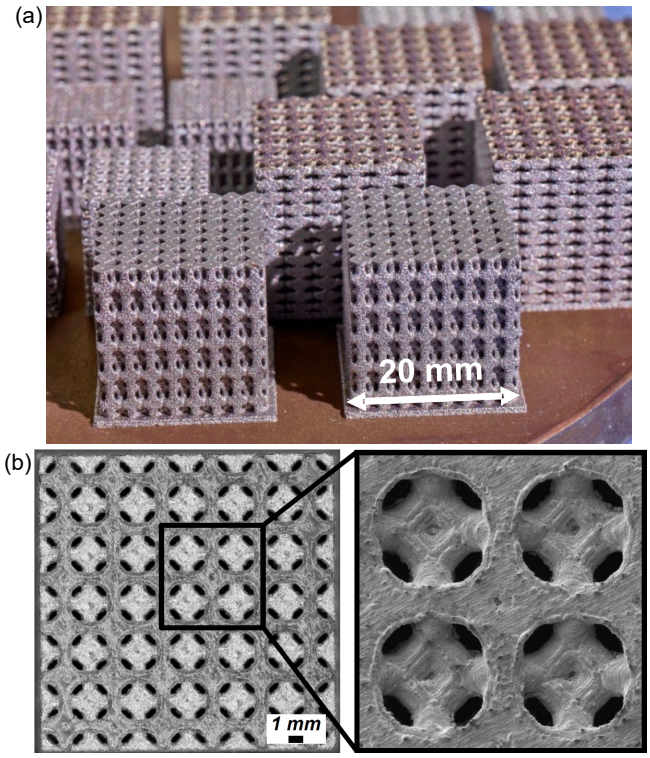

Figure 6: W lattice structure samples fabricated by means of LPBF.

Plasma limiter PFCs for DEMO are currently being investigated as components that are foreseen to baffle intense transient heat pulses to the reactor walls in order that blanket structures behind these limiter components are not thermally overloaded or damaged. Transient wall loadings in a DEMO reactor can e.g. arise due to plasma instabilities which in turn can induce short but intense heat loadings on the order of several tens of $\mathrm{GW\,m^{-2}}$ for time periods of a few ms [20]. These extreme heat flux densities can damage the blanket structures of a reactor severely which means that specific sacrificial high heat flux component solutions are needed to avoid breaching fo the first wall which has a steady state heat load operating limit of approximately $1\,\mathrm{MW\,m^{-2}}$.

In this context, DEMO limiter PFCs must fulfil conflicting requirements: adequate heat exhaust capability and thermal conduction during steady state loading but sufficiently low thermal diffusivity during transient loading. A possible material solution for such limiter PFCs is hence the use of tailored porous W materials which can exhibit defined effective thermophysical properties - like overall mass density, specific heat or thermal conductivity - in combination with the beneficial plasma-wall interaction properties of W. Figure 6 indicates that LPBF can potentially serve as a possible fabrication route for such tailored and porous W materials.

4. Tungsten-copper composites

W-Cu composite materials are currently of interest as advanced heat sink materials for actively water-cooled divertor PFCs with potentially improved properties compared to existing Cu alloys, especially under fusion neutron irradiation [5, 21, 22, 23]. W-Cu composite materials can be fabricated through liquid Cu infiltration of open porous W preforms. By means of AM, tailored W structures can be fabricated as preforms for liquid Cu infiltration in order that tailored W-Cu composite structures can be realised as has been shown for a W-Cu composite based on a thin-walled W honeycomb structure in [7].

Apart from that, *finite element* (FE) based material distribution optimisation computations indicate that tailored W-Cu material distributions can reduce thermally induced stresses in high heat flux loaded divertor PFCs significantly [24]. In this context, efforts regarding the realisation of a PFC mock-up based on a tailored and additively manufactured W preform were undertaken. The result is shown in Figure 7. Figure 7a shows an additively manufactured W preform built onto bulk W PFM tiles by means of LPBF. The preform was built on an Aconity*ONE* LPBF facility, located at Fraunhofer IGCV, 86159 Augsburg, Germany. Spheroidised W powder as illustrated in Figure 2a (supplier: Tekna Advanced Materials Inc., product name: W -25) was used as raw material. In a subsequent fabrication step, the preform as illustrated in Figure 7a was melt infiltrated with Cu for the formation of a W-Cu composite structure heat sink (infiltration performed by Louis Renner GmbH, 85232 Bergkirchen, Germany). In Figure 7b, this assembly is shown after machining to final dimensions. The additively manufactured W preform used for the fabrication of the mock-up illustrated in Figure 7b was a graded honeycomb structure exhibiting a varying wall thickness along the building direction in order to realise a higher W volume fraction at the joint to the W PFM tiles. The quality of the joining between the bulk W PFM tiles and the W-Cu heat sink part is expected to be high for such a design as the additively manufactured W is attached to the bulk W tiles due to the LPBF process and immersed into the Cu matrix of the heat sink.

5. Thermal shock experiments in JUDITH 2

As mentioned above, W is currently considered the preferred PFM for future magnetic confinement thermonuclear fusion devices. However, one particularly critical aspect in this regard is the behaviour of W under thermal shock loading. In a tokamak type fusion reactor, such loadings can impinge on divertor PFC surfaces due to so-called *edge localised modes* (ELMs) which are plasma edge instabilities that induce heat loads on the order of $\mathrm{GW\,m^{-2}}$ during time periods of a few ms [25]. The behaviour of W under such thermal shock loads is hence of crucial importance. In order to get insights whether a W material prepared by means of LPBF is applicable in highly loaded PFCs corresponding W samples were thermal shock tested in the electron beam facility JUDITH 2, located at Forschungszentrum Jülich [26, 27]. Within these high pulse number tests (1×10^5 thermal shocks), the damage behaviour and thermal performance of W prepared by LPBF was compared to that of W manufactured by classical metallurgical means (sintering and forging).

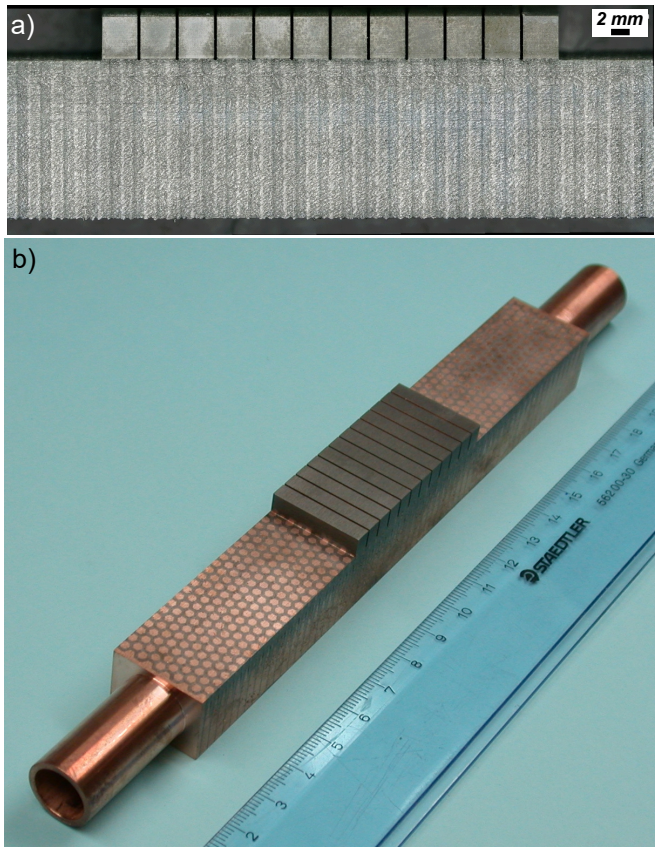

Figure 7: PFC mock-up based on an additively manufactured W preform fabricated by means of LPBF; (a) W honeycomb preform attached to bulk W PFM tiles, (b) PFC mock-up after Cu infiltration and machining to final dimensions.

This testing is considered highly relevant as W material consolidated by means of LPBF typically exhibits microcrack defects after the fabrication throughout the material as has been described within several references [7, 11, 12, 13, 14, 15, 16, 28, 29, 30, 31].

For the tests, bulk samples with dimensions of ca. 12 x 12 x 5 $\mathrm{mm^3}$ were cut from additively manufactured W consolidated by means of LPBF. Two different sample types were used that were fabricated with differing laser exposure parameters and substrate preheating (LPBF-W-1 sample fabricated with suitable parameters: laser power 400 W, scanning speed $510\,\mathrm{mm\,s^{-1}}$, hatch spacing 80 µm, layer thickness 40 µm, substrate preheating 1000 °C; LPBF-W-2 sample fabricated with rather inadequate parameters that yielded a material with increased porosity: laser power 375 W, scanning speed $210\,\mathrm{mm\,s^{-1}}$, hatch spacing 80 µm, layer thickness 40 µm, substrate preheating 600 °C). The LPBF facility used for the sample fabrication was an Aconity*ONE*, located at Aconity3D GmbH, 52134 Herzogenrath, Germany. Furthermore, a bulk conventionally manufactured pure W reference sample (Plansee SE, Austria; single forged and recrystallised at 1600 °C for 1 h) was included in the tests and analyses. Prior to the tests, all samples were grinded and polished to create a mirror like surface finish. The prepared samples were then soldered with a Ag-Cu braze on actively cooled Cu holders. The cooling circuit of JUDITH 2 was operated with a water temperature of 70 °C, a pressure of 20 MPa and a flow velocity of about $25\,\mathrm{m\,s^{-1}}$. During the exposure, electron beam pulses with power densities ranging from $0.14\,\mathrm{GW\,m^{-2}}$ to $0.55\,\mathrm{GW\,m^{-2}}$ (assuming a power absorption of 0.55 by W) were applied for a duration of 0.48 ms and with a repetition frequency of 25 Hz in order to simulate typical expected ELM loads. For an easier comparison of different exposure times and power densities of transient heat loads, it is useful to define a *heat flux factor* (HFF):

$$F_{HF} = L \times \sqrt{t} \tag{1}$$

with L being the applied power density (in $\mathrm{MW\,m^{-2}}$) and t the duration (in s). For convenience and better readability the unit $\mathrm{MW\,m^{-2}}\ \sqrt{\mathrm{s}}$ is typically omitted. Regarding short electron beam pulses, the HFF is proportional to the temperature increase and thus to the thermal stresses induced during the transient loading [32, 33]. For the experiments described within the present paper, HFFs of 3 (corresponding to a loading of $0.14\,\mathrm{GW\,m^{-2}}$ or $0.07\,\mathrm{MJ\,m^{-2}}$), 6, 9 and finally 12 (corresponding to a loading of $0.55\,\mathrm{GW\,m^{-2}}$ or $0.26\,\mathrm{MJ\,m^{-2}}$) were applied. Apart from that, a base temperature of 700 °C was achieved by applying an additional steady state heat load of $10\,\mathrm{MW\,m^{-2}}$ which by itself causes no surface modifications on tungsten [26]. Every 1×10^3 pulses (or 40 s) the tests were interrupted for 20 s allowing the test component to cool down and thus 100 on/off cycles were imposed on the samples. During exposure, the surface temperature was monitored by an *infrared* (IR) camera and a two-colour pyrometer. First, a comparison was made at low intensity thermal shocks (HFF 3) between the three different W grades under investigation, followed by a study of the damage progression in the LPBF W material with higher mass density (up to HFF 12).

In order to illustrate the thermal performance of the

tested samples, the change of the surface temperature (measured by IR and assuming an emissivity of 0.2) during the transient tests with HFF 3 is shown in Figure 8 relative to the first cycle. This relative representation was chosen as the emissivity of W surfaces is notably influenced by surface defects such as cracking or roughening which means that an accurate assessment of absolute temperature values would not be that meaningful.

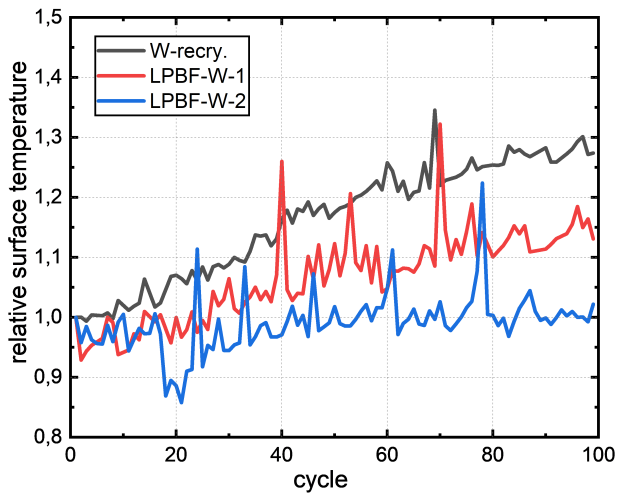

Figure 8: Progression of the relative change in surface temperature during transient electron beam tests with HFF 3 for different W samples.

The spikes that are visible in the curves in Figure 8 are due to the fact that the transient loading and the IR thermogramme recording are not synchronised, so the time between the impinging of one transient and the IR measurement varies. However, it can be seen that overall there is a slight increase in measured surface temperature. This, however, is not attributed to a reduction in thermal conductivity. Rather, this is attributed to surface modifications that evolve during the loading which in turn change the emissivity of the surfaces. This can be concluded as the change is highest for the reference W with its, in the beginning, defect free surface. Furthermore, the increase in the relative surface temperature is less for the additively manufactured LPBF W samples which is attributed to their higher emissivity already at the beginning of the experiments due to the presence of porosity and microcracks. Hence, Figure 8 illustrates that the thermal performance of W prepared by LPBF seems to be comparable to that of conventionally manufactured W. Apart from that, it is important to mention that no significant changes during or after the tests were observed regarding the cool down behaviour of the tested samples.

In Figure 9, macroscopic images of a LPBF W sample before (Figure 9a) and after (Figure 9b) thermal shock testing are illustrated. The sample was loaded with 1×10^5 HFF 12 transients, i.e. the highest applied loadings. It can be seen that from a macroscopic point of view some surface modification is visible although the material appears intact without loss of material or extensive crack defects. This indicates that W prepared by means of LPBF can exhibit sufficient mechanical integrity in order to cope with harsh thermal shock loads.

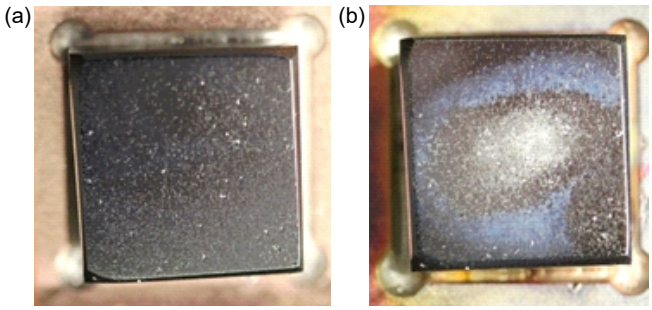

Figure 9: Macroscopic images of a LPBF W sample (a) before and (b) after electron beam loading with 1×10^5 HFF 12 transients.

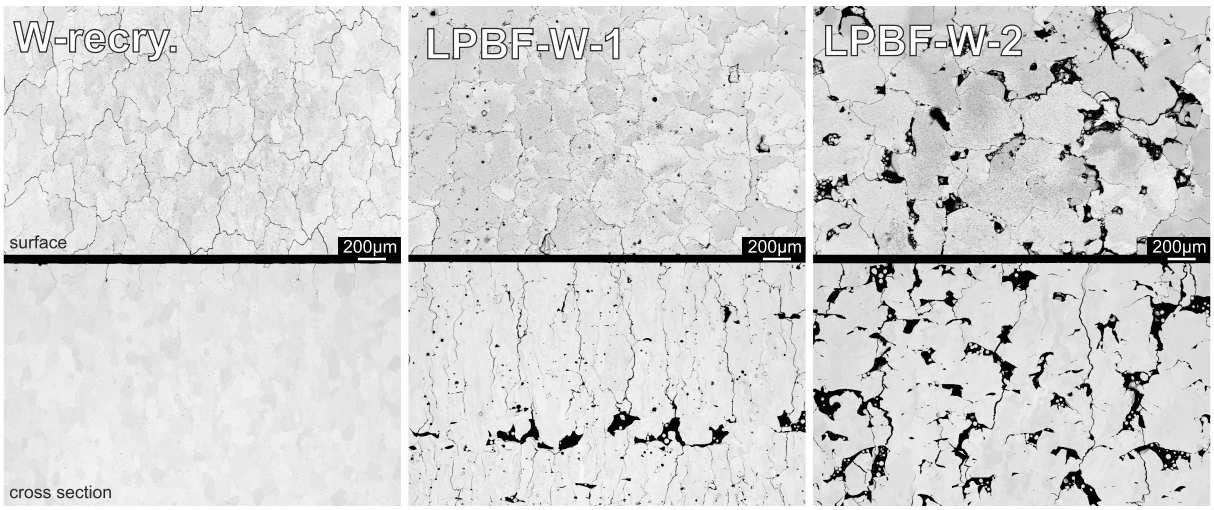

Figure 10: SEM images of surfaces and cross sections of the three different tested W grades loaded with 1×10^5 HFF 3 transients.

In Figure 10, SEM images of surfaces and cross sections of the three different tested W grades loaded with 1×10^5 HFF 3 transients are shown. It can be seen that the recrystallised reference W exhibits cracks on the loaded surface with a depth of about up to 200 µm. In the LPBF W samples, cracks are omnipresent throughout the material but no significant difference could be identified between the loaded and unloaded areas. Furthermore, it should be noted that the LPBF-W-1 sample exhibits a defective layer with higher porosity inside the material in a depth of about 1 mm probably due to a disturbance during the layer build-up process. Apart from that, it can be seen that the LPBF-W-2 sample exhibits considerably more porosity than the LPBF-W-1 sample. In terms of mechanical and thermophysical properties the LPBF-W-1 sample is certainly preferable for high heat flux PFC applications due to its higher mass density. For the further damage progression test series we hence limited our experiments to this material.
In Figure 11, SEM images of surfaces and cross sections of three LPBF-W-1 samples which were loaded with increasingly intense thermal shocks (HFF 3, HFF 6 and HFF 12, each 1×10^5 pulses) are shown. The cross sections on the left and in the middle show again the faulty layer in a depth of about 1 mm which however does not seem to lead to unacceptable damage at the sample surface.

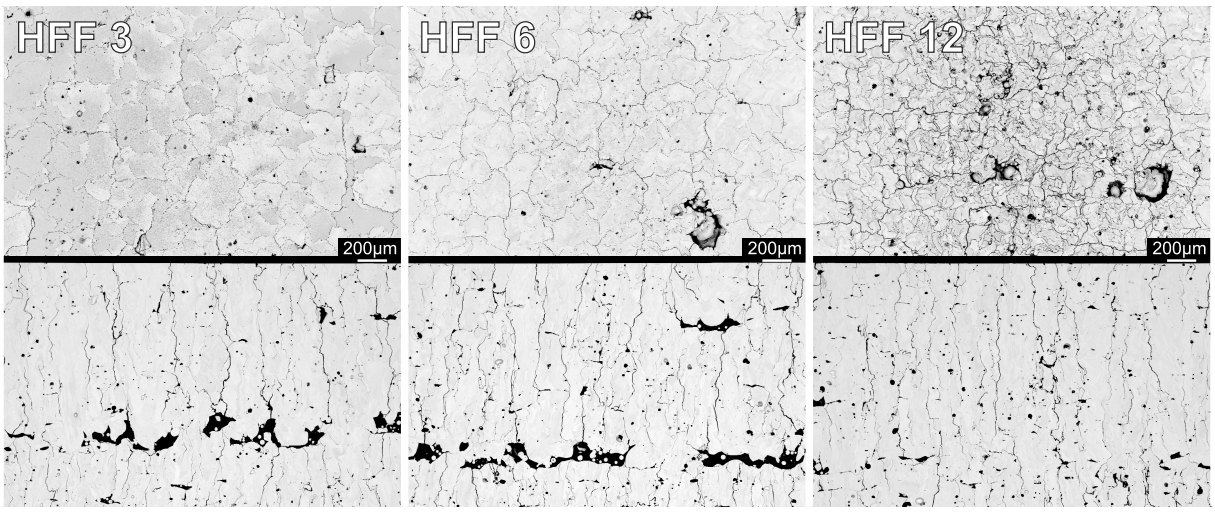

Figure 11: SEM images of surfaces and cross sections of LPBF-W-1 samples loaded with increasingly intense thermal shocks (HFF 3, HFF 6 and HFF 12, 1×10^5 transients each).

Figure 11 illustrates a distinctive damage evolution meaning that more and new cracks can be identified on the sample surfaces with increasing HFF. Within the cross sections of the samples, however, it is not possible to differentiate between cracks caused by the thermal shock loading and the ones which were present from the beginning due to the LPBF processing.
In reference [34], high pulse number thermal shock tests with the same intensity, number and base temperature as reported within the present paper (HFF 12) were conducted on an ITER-grade W material and many newly developed W alloys produced by *powder injection molding* (PIM). Not all of them could sustain the applied thermal shocks without macroscopic damage, illustrating the high potential and thermal shock resistance of W fabricated by means of LPBF.

6. Conclusions

Within the present paper, recent progress regarding AM of pure W by means of LPBF was discussed. In this context, several aspects were highlighted: First, the influence of the raw powder material characteristics on the additive fabrication process and the resulting W part quality was shown. In this regard, it was found that there is a strong influence of the powder characteristics on the built part quality and that as expected spheroidised W powders are best suited for LPBF processing as has also been found by other authors [35, 36]. In particular, it was in this respect pointed out that thin-walled test parts exhibited distinct differences in built part quality in terms of porosity and surface quality depending on the type of raw powder material used. Furthermore, examples of complexly shaped W lattice structure samples fabricated by means of LPBF were illustrated. These anisotropic lattices demonstrate that also for pure W it is possible to exploit the design freedom that is offered by AM processes. Apart from that, the application of an additively manufactured W structure as preform for a W-Cu composite was demonstrated which illustrates that tailored W-Cu composite structures can be realised with the help of AM. Finally, thermal shock experiments on bulk W samples consolidated by means of LPBF were discussed. These experiments demonstrated that W material consolidated by means of LPBF is capable of surviving intense thermal shock loads. This is an encouraging result indicating that the thermal performance and stability of W fabricated by means of LPBF is comparable to

conventionally fabricated W despite the presence of microcrack defects that typically occur in W consolidated through LPBF. In turn, this implies that the further investigation of additively manufactured W consolidated by means of LPBF with regard to applications in highly loaded PFCs of future magnetic confinement thermonuclear fusion devices can be considered worthwhile.

Acknowledgement

This work has been carried out within the framework of the EUROfusion Consortium and has received funding from the Euratom research and training programme 2014-2018 and 2019-2020 under grant agreement No 633053. The views and opinions expressed herein do not necessarily reflect those of the European Commission.
Apart from that, the authors want to acknowledge Pierluigi Fanelli and Riccardo De Luca, University of Tuscia, as well as Francesco Vivio, University of Rome Tor Vergata, for providing CAD files for the lattices that are illustrated in Figure 6 of the present paper. Volker Rohde, IPP Garching, is acknowledged for taking photographs of the W lattice samples that are illustrated in Figure 6 of the present paper. Moreover, Louis Renner GmbH is acknowledged for performing the Cu infiltration of the specimen illustrated in Figure 7b of the present paper.

References

[1] S. Gorsse et al., Additive manufacturing of metals: a brief review of the characteristic microstructures and properties of steels, Ti-6Al-4V and high-entropy alloys, Science and Technology of Advanced Materials 18 (1) (2017) 584–610. doi:10.1080/14686996.2017.1361305.

[2] T.S. Srivatsan and T.S. Sudarshan, Additive manufacturing: Innovations, advances, and applications, CRC Press, 2016.

[3] J. Roth et al., Recent analysis of key plasma wall interactions issues for ITER, Journal of Nuclear Materials 390-391 (2009) 1–9. doi:https://doi.org/10.1016/j.jnucmat.2009.01.037.

[4] R. Neu et al., Tungsten fibre-reinforced composites for advanced plasma facing components, Nuclear Materials and Energy 12 (2017) 1308–1313. doi:10.1016/j.nme.2016.10.018.

[5] A. v. Müller et al., Melt infiltrated tungsten-copper composites as advanced heat sink materials for plasma facing components of future nuclear fusion devices, Fusion Engineering and Design 124 (2017) 455–459. doi:10.1016/j.fusengdes.2017.01.042.

[6] A. v. Müller et al., Microstructural investigations of tungsten manufactured by means of laser beam melting, Proceedings of the 6th International Conference on Additive Technologies, ISBN 978-961-285-537-6 (2016) 61–66.

[7] A. v. Müller et al., Additive manufacturing of pure tungsten by means of selective laser beam melting with substrate preheating temperatures up to 1000 °C, Nuclear Materials and Energy 19 (2019) 184–188. doi:10.1016/j.nme.2019.02.034.

[8] D. Wang et al., Dense Pure Tungsten Fabricated by Selective Laser Melting, Applied Sciences 7 (4) (2017) 430. doi:10.3390/app7040430.

[9] A. Iveković et al., Selective laser melting of tungsten and tungsten alloys, International Journal of Refractory Metals and Hard Materials 72 (2018) 27–32. doi:https://doi.org/10.1016/j.ijrmhm.2017.12.005.

[10] C. Tan et al., Selective laser melting of high-performance pure tungsten: parameter design, densification behavior and mechanical properties, Science and technology of advanced materials 19 (2018) 370–380. doi:https://doi.org/10.1080/14686996.2018.1455154.

[11] D.-Z. Wang, K.-L. Li, C.-F. Yu, J. Ma, W. Liu, Z.-J. Shen, Cracking Behavior in Additively Manufactured Pure Tungsten, Acta Metallurgica Sinica (English Letters) 32 (2019) 127–135. doi:10.1007/s40195-018-0752-2.

[12] A.T. Sidambe, Y. Tian, P.B. Prangnell, P. Fox, Effect of processing parameters on the densification, microstructure and crystallographic texture during the laser powder bed fusion of pure tungsten, International Journal of Refractory Metals and Hard Materials 78 (2019) 254–263. doi:https://doi.org/10.1016/j.ijrmhm.2018.10.004.

[13] M. Guo, D. Gu, L. Xi, H. Zhang, J. Zhang, J. Yang, R, Wang, Selective laser melting additive manufacturing of pure tungsten: Role of volumetric energy density on densification, microstructure and mechanical properties, International Journal of Refractory Metals and Hard Materials 84 (2019) 105025. doi:10.1016/j.ijrmhm.2019.105025.

[14] S. Wen, C. Wang, Y. Zhou, L. Duan, Q. Wei, S. Yang, Y. Shi, High-density tungsten fabricated by selective laser melting: Densification, microstructure, mechanical and thermal performance, Optics Laser Technology 116 (2019) 128–138. doi:10.1016/j.optlastec.2019.03.018.

[15] Z. Xiong, P. Zhang, C. Tan, D. Dong, W. Ma, K. Yu, Selective Laser Melting and Remelting of Pure Tungsten, Advanced Engineering Materials 22 (3) (2020) 1901352. doi:https://doi.org/10.1002/adem.201901352.

[16] J. Wright, Additive Manufacturing of Tungsten, PhD thesis, University of Sheffield (2020).

[17] B. Buschmann, Influence of Powder Characteristics and Component Wall Thickness on Material Quality when Producing Pure Tungsten by Means of Laser Powder Bed Fusion, Master's thesis, Technische Universität München (2019).

[18] R. De Luca et al., Preliminary investigation on W foams as protection strategy for advanced FW PFCs, Fusion Engineering and Design 146 (2019) 1690–1693. doi:https://doi.org/10.1016/j.fusengdes.2019.03.017.

[19] R. De Luca et al., Parametric design study of a substrate material for a DEMO sacrificial limiter, Fusion Engineering and Design 158 (2020) 111721. doi:https://doi.org/10.1016/j.fusengdes.2020.111721.

[20] F. Maviglia et al., Wall protection strategies for DEMO plasma transients, Fusion Engineering and Design 136 (2018) 410 – 414. doi:https://doi.org/10.1016/j.fusengdes.2018.02.064.

[21] D. Stork et al., Developing structural, high-heat flux and plasma facing materials for a near-term DEMO fusion power plant: The EU assessment, Journal of Nuclear Materials 455 (1-3) (2014) 277–291. doi:10.1016/j.jnucmat.2014.06.014.

[22] J.H. You et al., European divertor target concepts for DEMO: Design rationales and high heat flux performance, Nuclear Materials and Energy 16 (2018) 1–11. doi:https://doi.org/10.1016/j.nme.2018.05.012.

[23] A. v. Müller, B. Böswirth, V. Cerri, H. Greuner, R. Neu, U. Siefken, E. Visca, J.-H. You, Application of tungsten-copper composite heat sink materials to plasma-facing component mock-ups, Physica Scripta T171 (2020) 014015. doi:10.1088/1402-4896/ab4142.

[24] B. Curzadd et al., Topology optimization of tungsten/copper structures for plasma-facing component applications, Nuclear Fusion 59 (8) (2019) 086003. doi:10.1088/1741-4326/ab1ff5.

[25] A. Loarte et al., Chapter 4: Power and particle control, Nuclear Fusion 47 (6) (2007) S203–S263. doi:10.1088/0029-5515/47/6/s04.

[26] Th. Loewenhoff et al., Experimental simulation of Edge Localised Modes using focused electron beams – features of a circular load pattern, Journal of Nuclear Materials 415 (1, Supplement) (2011) S51 – S54. doi:https://doi.org/10.1016/j.jnucmat.2010.08.065.

[27] P. Majerus et al., The new electron beam test facility JUDITH II for high heat flux experiments on plasma facing components, Fusion Engineering and Design 75-79 (2005) 365 – 369. doi:https://doi.org/10.1016/j.fusengdes.2005.06.058.

[28] B. Vrancken, R. K. Ganeriwala, M. J. Matthews, Analysis of laser-induced microcracking in tungsten under additive manufacturing conditions: Experiment and simulation, Acta Materialia 194 (2020) 464–472. doi:https://doi.org/10.1016/j.actamat.2020.04.060.

[29] Z. Hu, Y. Zhao, K. Guan, Z. Wang, Z. Ma, Pure tungsten and oxide dispersion strengthened tungsten manufactured by selective laser melting: Microstructure and cracking mechanism, Additive Manufacturing 36 (2020) 101579. doi:10.1016/j.addma.2020.101579.

[30] J. Braun, L. Kaserer, J. Stajkovic, K.-H. Leitz, B. Tabernig, P. Singer, P. Leibenguth, C. Gspan, H. Kestler, G. Leichtfried, Molybdenum and tungsten manufactured by selective laser melting: Analysis of defect structure and solidification mechanisms, International Journal of Refractory Metals and Hard Materials 84 (2019) 104999. doi:10.1016/j.ijrmhm.2019.104999.

[31] K. Li, D. Wang, L. Xing, Y. Wang, C. Yu, J. Chen, T. Zhang, J. Ma, W. Liu, Z. Shen, Crack suppression in additively manufactured tungsten by introducing secondary-phase nanoparticles into the matrix, International Journal of Refractory Metals and Hard Materials 79 (2019) 158–163. doi:10.1016/j.ijrmhm.2018.11.013.

[32] T. Hirai and G. Pintsuk, Thermo-mechanical calculations on operation temperature limits of tungsten as plasma facing material, Fusion Engineering and Design 82 (4) (2007) 389 – 393. doi:https://doi.org/10.1016/j.fusengdes.2007.03.032.

[33] Y. Ueda et al., Baseline high heat flux and plasma facing materials for fusion, Nuclear Fusion 57 (9) (2017) 092006. doi:10.1088/1741-4326/aa6b60.

[34] Th. Loewenhoff et al., High pulse number thermal shock testing of tungsten alloys produced by powder injection molding, Nuclear Materials and Energy 20 (2019) 100680. doi:https://doi.org/10.1016/j.nme.2019.100680.

[35] X. Zi, C. Chen, X. Wang, P. Wang, X. Zhang, K. Zhou, Spheroidisation of tungsten powder by radio frequency plasma for selective laser melting, Materials Science and Technology 34 (6) (2018) 735–742. doi:10.1080/02670836.2017.1410955.

[36] A.T. Sidambe, D.S. Judson, S.J. Colosimo, P. Fox, Laser powder bed fusion of a pure tungsten ultrafine single pinhole collimator for use in gamma ray detector characterisation, International Journal of Refractory Metals and Hard Materials 84 (2019) 104998. doi:10.1016/j.ijrmhm.2019.104998.